THE ASTROPHYSICAL JOURNAL, 205: 82–93, 1976 April 1

CYANOACETYLENE IN DENSE INTERSTELLAR CLOUDS

M. MORRIS
Owens Valley Radio Observatory, California Institute of Technology
B. E. TURNER
National Radio Astronomy Observatory*
PATRICK PALMER
University of Chicago
AND
B. ZUCKERMAN†
University of Maryland
Received 1975 July 7; revised 1975 September 9

ABSTRACT

Cyanoacetylene (H—C≡C—C≡N) has been detected in 17 galactic sources, including six clouds in the vicinity of the galactic center, nine clouds associated with H II regions and/or far-infrared sources, one dark dust cloud, and the molecular envelope of a carbon star. Seven rotational transitions between $J = 5 \rightarrow 4$ and $J = 14 \rightarrow 13$ were studied. An extensive map of the $5 \rightarrow 4$ line in the Sgr B2 cloud shows the presence of a nearby second cloud at much lower velocities than the main cloud.

Statistical equilibrium calculations were performed and matched to the observations of several sources. These calculations indicate the following: (1) homogeneous cloud models are inadequate for at least one source, Sgr B2, for which a two-component (core-halo) model is presented; (2) the observed lines of HC_3N are usually, if not always, optically thin; (3) fairly high densities ($\gtrsim 10^4$ cm^{-3}) are generally required to account for the observed lines; (4) the $J = 1 \rightarrow 0$ transition of HC_3N in Sgr B2 is probably a weak maser. Several sources are discussed individually.

Subject headings: interstellar: molecules — masers — radio sources: lines

I. INTRODUCTION

Interstellar cyanoacetylene (HC_3N) was discovered by Turner (1971), who detected emission in the $J = 1 \rightarrow 0$ line toward Sgr B2. Since then several additional transitions have been detected in Sgr B2 (Morris *et al.* 1973*a*, hereinafter referred to as Paper I; Dickinson 1972), the emission has been mapped in Sgr B2 (Paper I; McGee *et al.* 1973, hereinafter referred to as MNBK; McGee, Newton, and Butler 1975), and several new sources have been reported (Paper I). However, cyanoacetylene has not, until now, been used as a probe of the physical conditions in regions where it is found.

Cyanoacetylene is useful for studying dense interstellar clouds for several reasons. First, because it is a linear molecule with a closed-shell electronic configuration, the rotational energies are determined solely by end-over-end rotation: $E_J \propto J(J + 1)$ (ignoring hyperfine splittings, which are astrophysically important for only the lowest levels—$J \lesssim 3$). Thus the spectrum is simple, and allowed transitions connect only adjacent levels. Second, because it is relatively massive (HC_3N has more "heavy" atoms that any other widespread interstellar molecule), the rotational constant is small ($B_0 = 4.55$ GHz), and the spectrum is compressed in frequency relative to lighter molecules. For example, HC_3N has 10 times as many transitions in a given frequency range as has HCN. Thus a wealth of information is potentially available for studying the excitation of HC_3N, and therefore for determining the physical conditions in the regions in which it is found. Finally, the abundances of HC_3N in interstellar clouds, although high enough that the molecule is easily observed in many sources, are low enough that the radio lines are usually optically thin. Radiative transfer does not complicate the analysis of HC_3N lines, and accurate observations can be interpreted with much less ambiguity than arises with optically thick lines. Another advantage of small optical depths is that observations of the three distinct ^{13}C-substituted species will allow an accurate determination of the $^{12}C/^{13}C$ abundance ratio.

In this paper, we present the results of a survey of interstellar cyanoacetylene involving seven rotational transitions ranging from $J = 5 \rightarrow 4$ to $J = 14 \rightarrow 13$. A total of 17 sources were detected, including six galactic center sources, nine sources associated with H II regions and/or far-infrared sources, one dark dust cloud, and the molecular envelope of a carbon star. In Sgr B2, the $J = 5 \rightarrow 4$ line has been mapped over a large region ($8' \times 14'$), showing the presence of

* The National Radio Astronomy Observatory is operated by Associated Universities, Inc., under contract with the National Science Foundation.

† Alfred P. Sloan Foundation Fellow.

two distinct clouds, and upper limits have been obtained for the $J = 10 \rightarrow 9$ lines from ^{13}C-substituted species. The observations are presented in § II, and several sources are discussed individually. Excitation calculations are discussed in § III and applied to five sources for which sufficient data exist. These calculations, and the data presented by MNBK, suggest that the intensity of the $1 \rightarrow 0$ line in Sgr B2 is the result of weak maser action.

II. OBSERVATIONS

The 36 foot (11 m) NRAO telescope at Kitt Peak was used to observe HC_3N during seven observing sessions between 1972 February and 1974 March. For all of the observations,[1] NRAO equipment was used,

[1] Data for the $J = 14 \rightarrow 13$ transition were kindly made available to us by Dr. Carl Gottlieb, who observed this line at the Millimeter Wave Observatory of the University of Texas.

TABLE 1

CYANOACETYLENE SURVEY DATA

Source (1)	Position (2)	(1950.0) (3)	Transition ($J \rightarrow J-1$) (4)	T_A (K) (5)	Δv (km s^{-1}) (6)	v_{LSR} (km s^{-1}) (7)	Month, Year (8)
W3(HCN)	02^{h}21^{m}47^s.0	+61°52′54″	10 → 9	0.46	7.5	−42.5 ± 0.8	1973 Feb.
W3(IRS-5)	02 21 53.2	+61 52 21	5 → 4	≤0.12	...	...	1974 May
Cloud 2	04 38 38.6	+25 35 00	5 → 4	1.19	0.62	+6.05 + 0.15	1974 May
Orion A (1′.2 W)	05 32 42.2	−05 24 20	5 → 4	0.32	2.9	+ 9.4 ± 1.5	1974 May
Orion A (1′.2 E)	05 32 51.8	−05 24 20	5 → 4	0.36	4.7	+ 9.8 ± 1.5	1974 May
Orion A (1′.2 N)	05 32 47.0	−05 23 08	5 → 4	0.66	3.3	+ 8.7 ± 1.5	1974 May
Orion A (1′.2 S)	05 32 47.0	−05 25 32	5 → 4	0.58	3.5	+ 6.3 ± 1.5	1974 May
Orion A (KL)	05 32 47.0	−05 24 20	5 → 4	0.64	4.5	+ 8.3 ± 1.5	1974 May
Orion A (KL)	05 32 47.0	−05 24 20	8 → 7	1.57	2.4	+ 9.9 ± 1.1	1972 Feb.
Orion A (KL)	05 32 47.0	−05 24 20	10 → 9	1.77	3.5	+ 7.7 ± 0.8	1973 Feb.
Orion A (KL)	05 32 47.0	−05 24 20	11 → 10	1.28	15.8?	+ 8.6 ± 1.8	1972 May
Orion A (KL)	05 32 47.0	−05 24 20	14 → 13	1.60	4.1	...	1974 May*
NGC 2264	06 38 25.0	+09 32 06	5 → 4	0.33?	5.9	+12.5 ± 3.0	1973 Oct.
IRC +10216	09 45 14.8	+13 30 39	5 → 4	0.21	26.4	−24.2 ± 3.0	1973 Oct.
IRC +10216	09 45 14.8	+13 30 39	8 → 7	0.84	27.8	−28. ± 4.0	1972 Feb.
IRC +10216	09 45 14.8	+13 30 39	10 → 9	0.95	26.1	−26.7 ± 1.5	1974 Mar.
IRC +10216	09 45 14.8	+13 30 39	12 → 11	0.70	25.4	−27.9 ± 2.7	1974 Apr.
NGC 6334N	17 17 32.0	−35 44 20	5 → 4	0.66	2.9	− 5.1 ± 1.6	1974 May
M17	18 17 30.0	−16 15 36	5 → 4	0.38	3.4	+18.6 ± 1.6	1974 May
G34.3 +0.1	18 50 47.0	+01 11 00	5 → 4	0.31	5.0	+57.6 ± 1.6	1974 May
W51	19 21 27.0	+14 24 30	5 → 4	0.18	15.5	+61.5 ± 2.0	1973 Oct.
W51	19 21 27.0	+14 24 30	8 → 7	≤0.30	...	...	1972 Feb.
W51	19 21 27.0	+14 24 30	9 → 8	0.36?	28.7	+56.0 ± 4.0	1972 Feb.
W51	19 21 27.0	+14 24 30	10 → 9	0.39	11.7	+58.4 ± 4.0	1973 Feb.
W51	19 21 27.0	+14 24 30	11 → 10	1.16	5.9	+52.2 ± 4.0	1972 May
W75N	20 36 50.0	+42 26 58	5 → 4	0.20?	2.1	+10.0 ± 0.7	1974 May
DR-21(OH)	20 37 14.0	+42 12 00	5 → 4	0.35	3.4	−2.8 ± 2.0	1973 Oct.
DR-21(OH)	20 37 14.0	+42 12 00	10 → 9	≤0.40	...	...	1973 Feb.
DR-21	20 37 14.0	+42 09 00	5 → 4	0.35	4.0	− 2.4 + 2.0	1973 Oct.
Galactic Center Region							
Sgr(NH_3A)	17 42 28	−29 01 30	5 → 4	0.79†	23.5	+27.6 ± 2.0	1973 Oct.
Sgr(NH_3A)	17 42 28	−29 01 30	8 → 7	1.29	15.3	+30.5 ± 4.1	1972 Feb.
Sgr(NH_3A)	17 42 28	−29 01 30	9 → 8	0.80	13.6	+25.2 ± 3.7	1972 Feb.
Sgr(NH_3A)	17 42 28	−29 01 30	10 → 9	0.71	24.6	+28.0 ± 4.0	1973 Feb.
Sgr B2	17 44 11.0	−28 22 30	5 → 4	2.05	24.5	+54.0 ± 1.5	1974 May
Sgr B2	17 44 11.0	−28 22 30	8 → 7	2.29	19.6	+59.0 ± 4.1	1972 Feb.
Sgr B2	17 44 11.0	−28 22 30	9 → 8	3.00	24.6	+58.7 ± 3.7	1972 Feb.
Sgr B2	17 44 11.0	−28 22 30	10 → 9	2.70	18.7	+60.5 ± 4.0	1973 Feb.
Sgr B2	17 44 11.0	−28 22 30	11 → 10	2.72	23.3	+58.0 ± 4.0	1972 May
Sgr B2	17 44 11.0	−28 22 30	12 → 11	2.57	19.4	+58.9 ± 2.0	1974 Apr.
Sgr B2	17 44 11.0	−28 22 30	14 → 13	2.84	14.8	+61.3 ± 0.9	1974 May*
Cloud 12	17 44 21.0	−28 14 08	5 → 4	0.27	26.1	+22.5 ± 2.0	1973 Oct.
Cloud 12	17 44 21.0	−28 14 08	5 → 4	0.31	23.5	+87.5 ± 2.0	1973 Oct.
Cloud 13	17 44 59.0	−28 12 08	5 → 4	0.23	25.9	+22.0 ± 2.0	1973 Oct.
Cloud 13	17 44 59.0	−28 12 08	5 → 4	0.20	37.7	+83.9 ± 2.0	1973 Oct.
Sgr(NH_3B)	17 45 41.0	−27 56 48	5 → 4	0.22†	22.4	+85.9 ± 2.0	1973 Oct.
Cloud 15	17 46 28.0	−27 28 01	5 → 4	0.23	18.6	+54.7 ± 2.0	1973 Oct.
Cloud 15	17 46 28.0	−27 28 01	5 → 4	0.12?	17.7	+183.9 ± 2.0	1973 Oct.

NOTE.—A question mark indicates uncertain or tentative result. * Gottlieb personal communication. † Uncertain because of large baseline curvature.

TABLE 2

UNSUCCESSFUL SEARCHES FOR HC_3N

Source	Position	(1950.0)	Transition ($J \rightarrow J-1$)	ΔT_{p-p}	Resolution (kHz)	Month, Year
W3(OH)	$02^h23^m17^s0$	+61°39′00″	5 → 4	0.40	100	1973 Oct.
W3(OH)	02 23 17.0	+61 39 00	8 → 7	2.10	250	1972 Feb.
W3(OH)	02 23 17.0	+61 39 00	10 → 9	1.16	250	1973 Feb.
NGC 1333	03 25 55.6	+31 10 10	5 → 4	0.90	100	1974 May
OMC-2	05 33 00.0	−05 12 34	5 → 4	1.05	100	1974 May
NGC 2024	05 39 13.5	−01 56 57	5 → 4	0.90	100	1974 May
S269	06 11 46.5	+13 50 35	5 → 4	0.90	100	1974 May
L134	15 50 54.0	−04 31 00	5 → 4	0.65	100	1974 May
Cloud 4(NH_3)	16 24 08.0	−24 28 00	5 → 4	0.65	100	1974 May
W31	18 06 24.0	−20 19 53	5 → 4	0.55	1200	1972 June*
W33N	18 11 47.0	−17 54 00	5 → 4	0.55	1200	1972 June*
W43	18 45 00.0	−02 00 00	5 → 4	0.25	250	1973 Oct.
R Cr A	18 58 27.3	−37 01 26	5 → 4	0.80	250	1973 Oct.
W49	19 07 49.0	+09 01 18	5 → 4	0.50	250	1973 May
W49	19 07 49.0	+09 01 18	10 → 9	1.60	1200	1972 May
K3-50	19 59 59.5	+33 26 01	5 → 4	0.80	250	1973 Oct.
OH 69.5–1.0	20 08 10.0	+31 22 41	5 → 4	0.45	250	1974 May
AFCRL 809-2992	20 27 34.5	+40 01 10	5 → 4	0.25	250	1973 Oct.
Cloud 1	22 27 47.0	+74 58 08	5 → 4	1.05	100	1974 May
NGC 7538	23 11 36.8	+61 11 48	5 → 4	0.20	250	1973 Oct.
NGC 7538	23 11 36.8	+61 11 48	10 → 9	0.40	1200	1973 Feb.
NGC 7538	23 11 36.8	+61 11 48	11 → 10	0.80	1200	1972 May

* Turner and Gammon, private communication.

and has been described by us elsewhere (Turner *et al.* 1973; Morris *et al.* 1974; Morris *et al.* 1975). Calibration procedures are also described in these references. For all of the 1974 observations, a standard chopper-wheel calibration method was used. The uncertainties (primarily calibration uncertainties) in the antenna temperatures are 50 percent for lines measured prior to 1973 October, and thereafter, 15 percent for lines with $T_A \geq 0.70$ K and 25 percent for lines with $T_A < 0.70$ K. T_A is the peak antenna temperature of the line $[T_A \equiv (c^2/2k\nu^2)I(\nu)]$ above the background continuum, corrected for atmospheric attenuation and antenna losses and averaged over the main beam of the telescope. The half-power beam width of the 36 foot telescope varies approximately inversely with J from 64″ for the $J = 12 \rightarrow 11$ line to 150″ for the $J = 5 \rightarrow 4$ line.

Frequencies for the HC_3N transitions were calculated from $\nu_{J,J-1} = 2B_0J - 4D_JJ^3$, where $B_0 = 4549.0580 \pm 0.0005$ MHz, and $D_J = 0.5439 \pm 0.0005$ kHz (DeZafra 1971). Values of B_0 for the ^{13}C-substituted species were taken from Westenberg and Wilson (1960).

Table 1 is a summary of the data for all sources in which HC_3N has been detected. The first four columns are self-explanatory. The peak antenna temperature (or upper limit) for each transition is given in column (5). Columns (6) and (7) list the full width at half-power and the radial velocity with respect to the local standard of rest (LSR), both in kilometers per second. The month and year of each observation are listed in column (9). Sources searched unsuccessfully for HC_3N are listed in Table 2. The first four columns are the same as in Table 1. Columns (5) and (6) list the peak-to-peak noise temperature (corrected for atmospheric absorption and antenna losses) and the bandwidth of the filters used for the determination. Column (7) gives the month and year of each observation.

a) Sagittarius B2

The source having the strongest lines of HC_3N, and consequently the best studied source, is Sgr B2. Figure 1 presents spectra of all of the lines that have been detected in this direction. Remarkably, all nine lines have about the same antenna temperature, 2–3 K. Because Sgr B2 is probably spatially extended in all transitions (Paper I; MNBK; and below), this result is intrinsic to the source and is not the result of variations in the beam filling factor. The mean LSR velocity of the line centroids is 59.8 km s^{-1}, but there is a suggestion in the spectra with the best frequency resolution and signal-to-noise ratio that the velocity of peak emission intensity shifts from 60–65 km s^{-1} for the $1 \rightarrow 0$ and $2 \rightarrow 1$ lines to 54–60 km s^{-1} for higher transitions. A possible explanation for this effect is discussed below.

McGee *et al.* (1975) have suggested the presence of four clouds in Sgr B2 having radial velocities of 80.2, 68.6, 60.5, and 49.3 km s^{-1}, all of which overlap along the line of sight. They base this result on a multiple-Gaussian fitting to the asymmetric $J = 1 \rightarrow 0$ HC_3N line and on a similar, independent suggestion of the presence in Sgr B2 of two or three clouds based upon high-resolution H_2CO observations (Rogstad, Lockhart, and Whiteoak 1974). However, the overlapping multiple cloud picture should be viewed with caution for

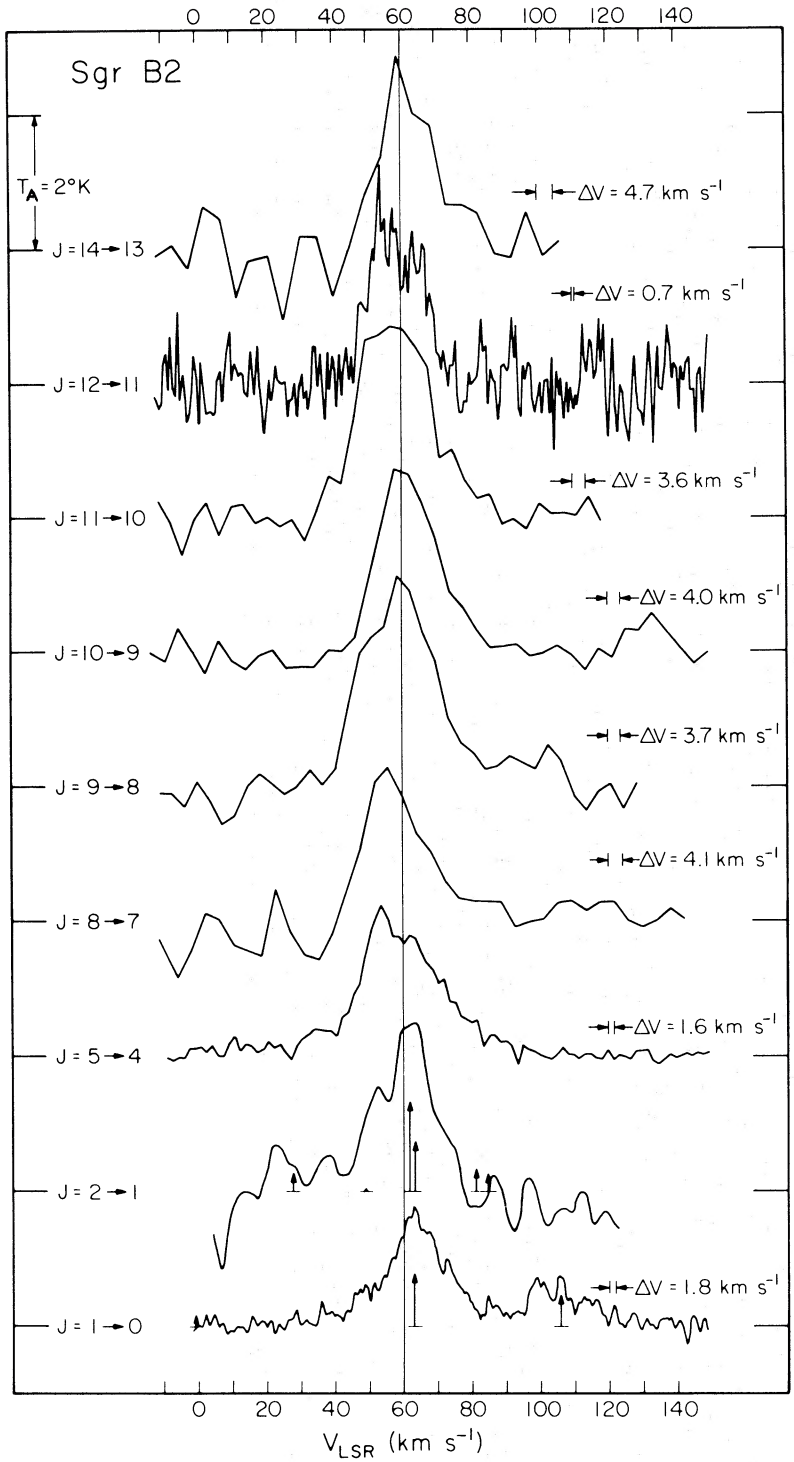

FIG. 1.—Cyanoacetylene lines observed to date in Sgr B2. The ordinate is antenna temperature corrected for atmospheric and antenna losses, and the abscissa is velocity with respect to LSR. All lines are drawn to the same scale. The velocity resolution is indicated above each spectrum for which it is available. The $J = 1 \rightarrow 0$ and $J = 2 \rightarrow 1$ spectra are taken from Turner (1971) and Dickinson (1972), respectively.

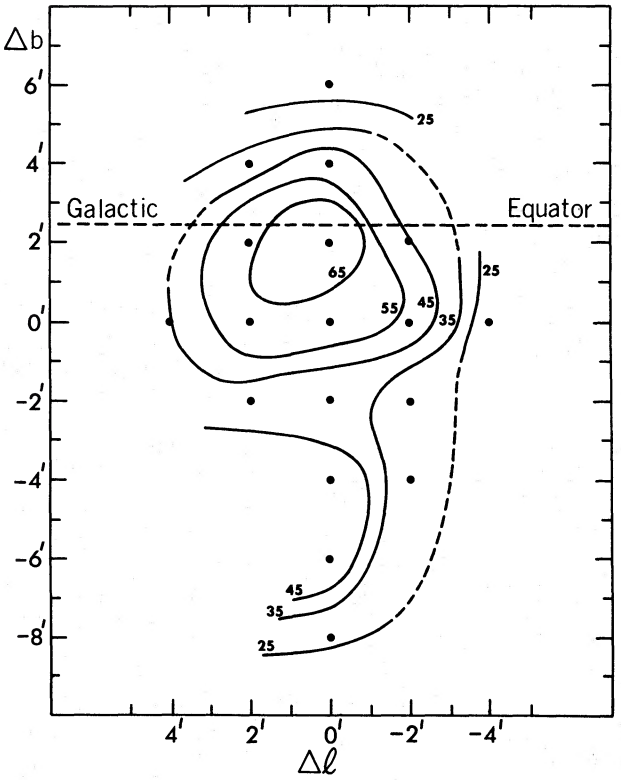

FIG. 2.—Map of integrated intensity of the $J = 5 \rightarrow 4$ HC_3N line in Sgr B2. Contour units are K-km s^{-1}. The points represent the positions at which spectra were taken. The 1950 coordinates of the reference position in Figs. 2–4 are the following: $\delta = 17^h44^m11^s0$, $\alpha = -28°22'30''$.

two reasons. First, in view of the complex velocity fields known to exist throughout the galactic center region, there is no *a priori* reason to expect that Gaussian line shapes are appropriate for the clouds which are seen in the direction of Sgr B2 (this is especially true for the $J = 1 \rightarrow 0$ line, which might have a non-Doppler line shape if it is indeed a weak maser as suggested in § III*c*). Second, the H_2CO absorption measured by Rogstad, Lockhart, and Whiteoak (1974) does not necessarily arise in the same regions as the HC_3N emission. We find no evidence supporting the overlapping multiple cloud model in the HC_3N observations presented in this paper, but higher spatial resolution ($\lesssim 30''$) observations are needed before any definite conclusions can be drawn. In order to keep our analysis simple, we assume below that HC_3N emission from the inner 2.5 of Sgr B2 is dominated by a cloud (or clouds) having a single velocity structure.

Within the uncertainties, the line width does not vary with J. This is noteworthy considering the several different beam sizes used. We conclude that Doppler broadening effects do not increase as the aperture increases from 1′ to 2.5. The HC_3N line widths are comparable with those of the nonmetastable lines of NH_3 in this source (~ 20 km s^{-1}), but are much smaller than those of metastable NH_3 lines (~ 40 km s^{-1}, Morris *et al.* 1973*b*). In fact, most of the complex molecules found in Sgr B2 have line widths of ~ 20 km s^{-1}.

Previous maps of the $8 \rightarrow 7$ line (Paper I) and the $1 \rightarrow 0$ line (MNBK) have shown that cyanoacetylene is extended over a large region about Sgr B2. We have mapped the $5 \rightarrow 4$ line over an $8' \times 14'$ region centered on Sgr B2 and have found emission at every point searched. The map of integrated intensity ($\int T_A dv$) is displayed in Figure 2. The $J = 5 \rightarrow 4$ emission from the main cloud peaks at the same place ($\Delta l \approx 0°$, $\Delta b \approx +2'$; see Fig. 2) and has about the same extent as $1 \rightarrow 0$ emission (MNBK). Within the resolution of the two maps, the shapes of the contours are also similar. The HC_3N intensity distribution is more extended than the 350 μ emission which presumably arises from cool (15–30 K) dust (Righini *et al.* 1975).

A second cloud about 7′ below the galactic plane, suggested by the integrated intensity map (Fig. 2), shows up distinctly in the velocity-latitude strip map through the source center (Fig. 3), its radial velocity (32 km s^{-1}) being quite different from that of the main Sgr B2 cloud. The 32 km s^{-1} HC_3N cloud might be associated with OH cloud 43 (McGee 1970) and H_2CO cloud 12 (Scoville, Solomon, and Thaddeus 1972). Figure 4, the velocity-longitude plot of Sgr B2 in the $5 \rightarrow 4$ line, shows some evidence for the lower velocity emission at the greater longitudes.

The two clouds in Figure 3 might be close to each other only in projection, but it is interesting to consider the possibility that they are bound gravitationally to each other. If the clouds are both at a distance of 10 kpc, if the radial velocity difference is assumed to be their total relative velocity, and if the projected separation (20 pc) is within a factor of 2 of their actual separation, then the combined masses of the two clouds must be $\sim 5 \times 10^6 M_\odot$ if the clouds are to be gravitationally bound. The mass of the Sgr B2 molecular cloud alone may be this large (Morris *et al.* 1973*b*, and below), so the existence of a binary cloud is entirely possible.

A search for the $10 \rightarrow 9$ transitions of the ^{13}C-substituted species of HC_3N in Sgr B2 yielded the following upper limits on intensity relative to the intensity of the same transition of the main species: $H^{13}C^{12}C^{12}CN$: ≤ 0.05, $H^{12}C^{13}C^{12}CN$: ≤ 0.05, and $H^{12}C^{12}C^{13}CN$: ≤ 0.04. If no differential fractionation has occurred, and if the excitation temperatures are the same for all isotopic species (a good assumption for small optical depths; see § III), these values become upper limits to the $[^{13}C]/[^{12}C]$ ratio. These results are in agreement with the $[^{12}C]/[^{13}C]$ ratio (36 ± 5) found by Gardner and Winnewisser (1975*b*) for the $1 \rightarrow 0$ transition if the optical depth of the main $10 \rightarrow 9$ transition is ≤ 1. The $9 \rightarrow 8$ transition of $H^{12}C^{12}C^{13}CN$ is coincident within the uncertainties with U81.541 (Solomon *et al.* 1973), but our negative result for the next higher transition, and the fact that the $9 \rightarrow 8$ transition of $H^{12}C^{13}C^{12}CN$ was not observed in the same spectrum, makes this an unlikely identification.

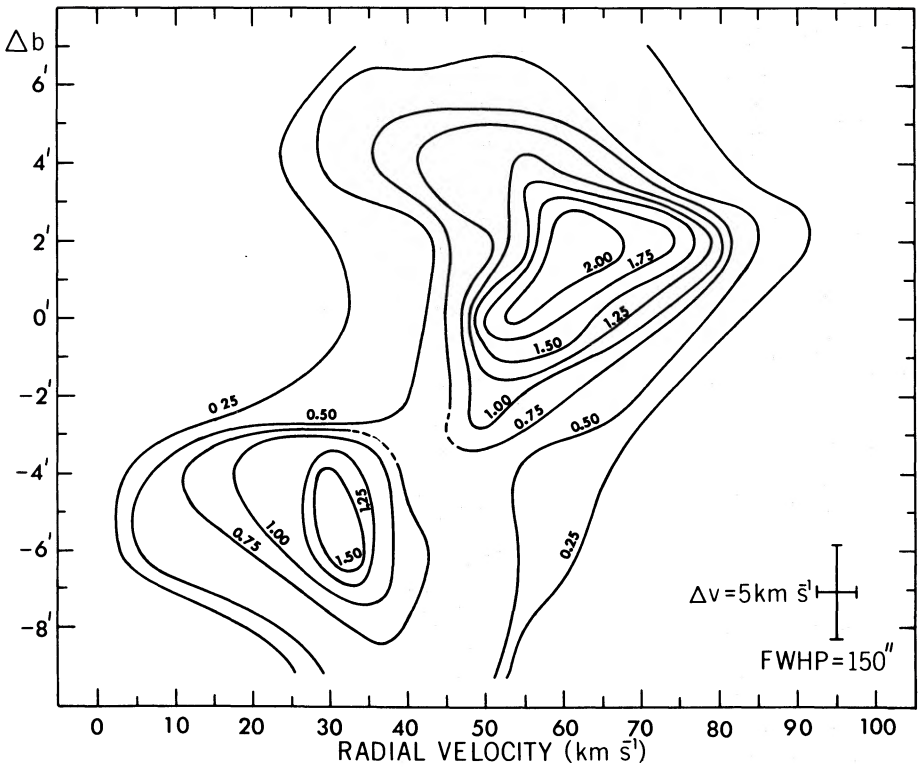

FIG. 3.—Velocity-latitude map of $J = 5 \rightarrow 4$ HC_3N emission in Sgr B2. Contour units are K antenna temperature. The spatial and velocity resolution are indicated on the figure.

b) Other Galactic Center Clouds

HC_3N has been detected in five galactic center clouds other than Sgr B2: Sgr(NH_3A), Sgr(NH_3B), and H_2CO clouds 12, 13, and 15. In all but Sgr (NH_3A), the HC_3N velocities and line widths are similar to those of H_2CO (Scoville, Solomon, and Thaddeus 1972) and NH_3 (Morris *et al.* 1973*b*; Kaifu *et al.* 1975). Cloud 12 refers to the 22 km s^{-1} velocity component, which is actually present at both positions listed in

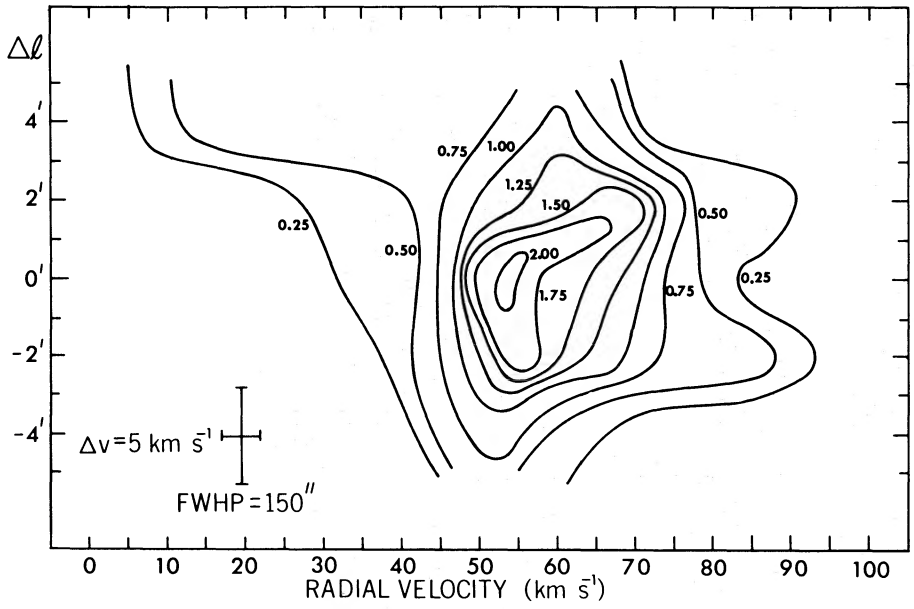

FIG. 4.—Velocity-longitude map of $J = 5 \rightarrow 4$ HC_3N emission in Sgr B2

Table 1 as clouds 12 and 13. Similarly, cloud 13 refers to the 85 km s^{-1} component, which extends over-positions listed as clouds 12 and 13, and Sgr (NH_3B).

In Sgr (NH_3A), the HC_3N line widths are significantly smaller than those of NH_3 and H_2CO (within the uncertainties, the widths of the different HC_3N lines are the same). The velocities of the HC_3N line maxima (25–30 km s^{-1}) coincide with those of NH_3, but are quite different from the peak H_2CO absorption velocity in this direction—46 km s^{-1}.

HC_3N has tentatively been detected in the cloud 15 direction with a velocity of 184 km s^{-1}. This direction and velocity coincide with those of an NH_3 feature found by Kaifu *et al.* (1975).

c) *Orion Molecular Cloud 1*

A total of five HC_3N lines have been detected in the direction of the Kleinmann-Low nebula (KL) in Orion (Table 1). In addition, a five-point map of $J = 5 \rightarrow 4$ emission was made with points separated by half a beamwidth (1'.2). HC_3N appears to be extended along the north-south ridge that is evident in emission from H_2CO (Evans *et al.* 1975), CS (Liszt *et al.* 1974), H_2S (Thaddeus *et al.* 1972), HCN (Clark, Buhl, and Snyder 1974), C_2H (Tucker, Kutner, and Thaddeus 1974), and CN (Turner and Gammon 1975). The radial velocities of HC_3N are consistent with the north-south velocity gradient of the Orion Molecular Cloud (Evans *et al.* 1975), but, unfortunately, the uncertainties in the measurements presented here are large. The weighted mean radial velocity of HC_3N lines at the KL position is 8.5 km s^{-1}, in close agreement with that of other molecules having extended emission about KL.

d) *Cloud 2*

At the position listed in Table 1 for Heiles's cloud 2 (the dark dust cloud in Taurus), Scoville (private communication) has found relatively deep and narrow 2 cm H_2CO absorption features. At this position, we have detected very narrow ($\Delta V \leq 1.0$ km s^{-1}) emission in the $5 \rightarrow 4$ line of HC_3N. The peak brightness temperature is uncertain because the line is unresolved, but is ~ 1.2 K averaged over 0.7 km s^{-1}. Three other dust cloud positions (L134, cloud 1, and cloud 4 [NH_3]) were searched for the $5 \rightarrow 4$ line without a detection. The cloud 2 detection makes cyanoacetylene the most complex molecule yet seen in a dark dust cloud.

e) *IRC +10216*

Four HC_3N transitions have been observed in the direction of the expanding molecular envelope surrounding the carbon star, IRC +10216. Figure 5 displays the $10 \rightarrow 9$ profile, which is flat-topped to within the noise. Morris (1975) has argued that a flat-topped profile from a spherical, uniformly expanding cloud implies an optically thin line. The interpretation of the HC_3N observations of this source (and upper limits to the ^{13}C species) has been discussed elsewhere (Morris *et al.* 1975), and an analysis of the

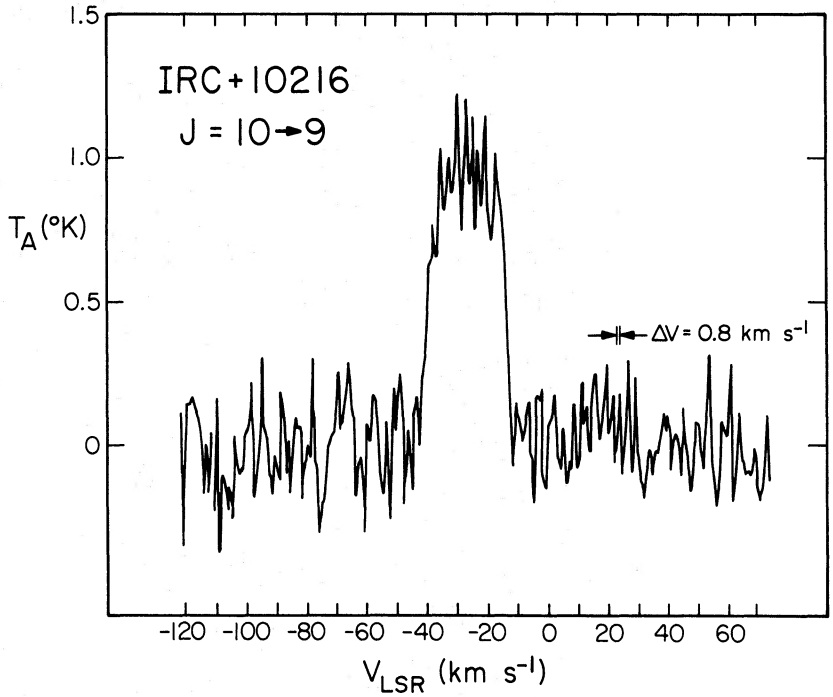

FIG. 5.—Spectrum of the $J = 10 \rightarrow 9$ transition of HC_3N in the molecular envelope surrounding IRC +10216. The ordinate is antenna temperature corrected for atmospheric and antenna losses, and the abscissa is LSR velocity.

molecular envelope based partially on these observations has been presented by Morris (1975). Therefore, we will not discuss this source further in this paper.

III. INTERPRETATION

a) Statistical Equilibrium Calculations

Equilibrium populations of the rotational levels of cyanoacetylene have been calculated for a variety of physical conditions in order to interpret the observations. These calculations included the effects of collisions with other particles, and the interaction of HC_3N molecules with the microwave radiation field.

In the initial calculations, the radiation field included the 2.7 K blackbody background plus transferred line radiation—that is, possible trapping of line photons was taken into account, assuming that large-scale motions in clouds account for the line widths. These calculations use the procedures described by Goldreich and Kwan (1974) and Scoville and Solomon (1974). For selection rules on collisions, we assumed that $|\Delta J| \leq 3$, that downward collisional transitions to all accessible sublevels are equally probable, and that detailed balancing holds. The lowest 20 levels (not including hyperfine splittings) were included. It was found that, for solutions that correspond to the observations, optical depths of HC_3N transitions are predicted to be too small (usually < 1) for trapping to have a significant effect.

A second set of calculations have been made which are similar to those described by Goldsmith (1972) and Turner *et al.* (1973). These calculations include (1) the lowest 25 levels, (2) interactions with the 2.7 K background (but line radiation is assumed not to affect the level populations), and (3) collisions, but, in this case, the cross sections for collisional transitions are more elaborate. Because of its axial symmetry, the HC_3N molecule is modeled as a "hard" ellipsoid of revolution, and the cross sections for rotational transitions induced by colliding point masses are calculated classically. This is done by solving the kinematic equations (conserving linear and angular momentum, and total kinetic energy) for an arbitrary angle of incidence, arbitrary impact parameter, and arbitrary relative velocity, and then integrating numerically over all angles, impact parameters, and a Maxwellian velocity distribution. To provide the correspondence with quantum-mechanical angular momentum states, the initial angular momentum is always a multiple of $\hbar$, and the final angular momenta are appropriately divided into intervals $\hbar$ wide. The lengths of the major and minor axes of the ellipsoid are crudely estimated by summing the van der Waals radii of the particles involved in the collision, giving a total interaction cross section for HC_3N of $\sim 4 \times 10^{-15}$ cm^{-2}. Collisions with both H_2 and He are considered, and the final collision rates are an abundance-weighted average of the rates for these two colliders ($[He]/[H_2] = 0.2$). The rates for each collider preserve detailed balancing, and tend to fall off slowly with ΔJ until $\Delta J \geq 4$, after which they decrease more rapidly.

The use of the classical correspondence for HC_3N is partially justified by the fact that the quantum numbers of the levels of interest are large (up to $J = 14$). However, this method of calculating collision rates is only meant as a rough estimate. The same calculations applied to HCN, for example, do not reproduce the preference for $\Delta J = 2$ transitions found by Green and Thaddeus (1974), although they do give grossly the same decrease of cross section with ΔJ (and, of course, small quantum numbers are involved, so the classical correspondence is not reliable for HCN). We did not consider hyperfine levels separately in this treatment.

The results of the statistical equilibrium calculations using the "hard-ellipsoid" collision rates are essentially similar to the results found initially with the simpler selection rules. Thus we believe that our conclusions are not very sensitive to the assumed cross sections. We have applied these calculations to several of the observed interstellar clouds in the following section.

b) Sagittarius B2: The Model

The observed brightness temperatures of the lines in Sgr B2 cannot be accounted for with a model consisting of a single, homogeneous cloud, even when the uncertainties in the measurements are taken into account. This fact is not surprising, since it is reasonable to expect that, in general, physical conditions vary continuously through a cloud. In order to keep the analysis simple, we have constructed a two-component model of Sgr B2 which is able to mimic the observations. More sophisticated models must await better spatial maps, smaller observational uncertainties, and more elaborate methods of analysis.

We have interpreted the two components as a core and a halo (a core-halo picture has often been discussed for Sgr B2), although the geometry will not be critical if the optical depths of the HC_3N lines are generally small (≤ 1) as our approximate calculations suggest. The parameters of the two cloud components are shown in Table 3.

A rather high density is found for the core ($n_T \approx 10^6$ cm^{-3}, where n_T is the total particle density). This value agrees with previous determinations of the core density (Zuckerman *et al.* 1971; Solomon *et al.* 1971). The core component dominates the intensity of HC_3N lines having $J_u \gtrsim 8$. On the other hand, the halo is about two orders of magnitude less dense, but accounts for about half of the intensity in the $J = 5 \rightarrow 4$ line and dominates for $J_u < 5$. The core-halo model is not very sensitive to the kinetic temperature, and thus a fairly wide range is allowed for both components. Table 3 indicates the most reasonable ranges. Present evidence suggests that T_k (the kinetic temperature) $\approx$20–40 K throughout the cloud (Cheung *et al.* 1969; Righini *et al.* 1975), and that the temperature rises to $\sim$100 K in the inner few parsecs of the core (Solomon *et al.* 1973).

Although the projected density of HC_3N [$N(HC_3N)$] is about the same in the two components, the fractional

TABLE 3

TWO-COMPONENT MODEL FOR SAGITTARIUS B2

Parameter	Core	Halo
log $[n_T(\mathrm{cm}^{-3})]$	6.0 ± 0.5	4.0 ± 0.7
T_k (K)	25–50	20–80
$N(HC_3N)\ \mathrm{cm}^{-2}$	$(2.0 \pm 0.4) \times 10^{14}$	$(1.8 \pm 0.8) \times 10^{14}$
D (pc)	7	15
log $[N(HC_3N)/N(H_2)]$	-11.0 ± 0.7	-9.4 ± 0.7
Mass $(M_\odot)$	$\sim 10^7$	$\sim 10^6$

abundance appears to be much higher in the halo. Depletion of HC_3N in the core may have occurred through a high rate of chemical reactions in the dense medium. In this regard, it is interesting that (*a*) HCN appears to have a relatively low abundance in Sgr B2 (Snyder and Buhl 1971), and (*b*) vinyl cyanide—a hydrogenated form of cyanoacetylene—has recently been detected in Sgr B2 with an estimated abundance comparable with that of HC_3N (Gardner and Winnewisser 1975*a*). Detection of CH_3CH_2CN in the core would provide further evidence that HC_3N goes to more complex forms.

The fractional abundances and cloud masses depend upon the value of the diameter, D, of each component. The diameter of the halo has been estimated from the extent of emission in the $J = 5 \rightarrow 4$ line (Fig. 2). The core diameter is derived from several consistent observations, which are the following, in order of decreasing relevance: (*a*) the extent of the CH_3CN emission (Solomon *et al.* 1973), (*b*) the extent of the $J = 8 \rightarrow 7$ HC_3N line (Paper I), (*c*) the size derived for the region emitting nonmetastable lines of NH_3 (Morris *et al.* 1973), (*d*) the extent of the 350 μ core (Righini *et al.* 1975), and (*e*) the size of the region emitting excited-state OH lines (Gardner, Ribes, and Sinclair 1971). The large mass of the core component in our model ($\sim 10^7\ M_\odot$) agrees with our previous estimate (Morris *et al.* 1973). If the core is highly clumped on a scale size $\lesssim 1$ pc, the mass in the core might be somewhat less than derived from our homogeneous cloud model. However, it is unlikely that the estimate of the core mass can be reduced by as much as an order of magnitude by the inclusion of clumping.

c) Sagittarius B2: The $J = 1 \rightarrow 0$ Transition: A Weak Maser

When selection rules for collisional transitions in linear molecules are such that dipole collisions do not dominate, the $J = 1 \rightarrow 0$ transition may have population inversion over a wide range of physical conditions (see, for example, Goldsmith 1972). This behavior has not yet been identified because the $1 \rightarrow 0$ lines of common linear molecules which might display it (CO, CS, and HCN) have large enough optical depths that the excitation is dominated by interaction with the radiation field. This is probably not the case with cyanoacetylene, however. Our statistical equilibrium calculations for HC_3N predict a population inversion for the $J = 1 \rightarrow 0$ transition roughly where $10^3 \lesssim n_T \lesssim 10^5\ \mathrm{cm}^{-3}$ and $T_k > 10$ K, and for the $J = 2 \rightarrow 1$ transition in a more restricted range of physical conditions. Therefore, it is theoretically reasonable to expect weak maser emission in the $1 \rightarrow 0$ line of HC_3N from the halo component of Sgr B2. In other sources, the column densities appear to be too small for a detectable line to occur.

The observations strongly imply that the $1 \rightarrow 0$ line is indeed masering weakly. The most compelling evidence for this is the following: (1) the intensity measured by McGee *et al.* (1975) is about a factor of 6 larger than can be accounted for in the above two-component model, or any similar model, in the absence of maser amplification. Assuming thermal emission, MNBK calculate $N(HC_3N) \approx 4 \times 10^{16}\ \mathrm{cm}^{-2}$ from the intensity of the $1 \rightarrow 0$ line (see McGee *et al.* 1975), but this projected density is ~ 100 times larger than that derived above from seven higher-lying cyanoacetylene lines. (2) The hyperfine intensity ratios reported by Turner (1971), and by MNBK (10:4:1 for the $F = 2 \rightarrow 1 : 1 \rightarrow 1 : 0 \rightarrow 1$ components), deviate from their LTE values (5:3:1) in the sense expected if maser amplification is occurring, since gain is proportional to line strength. Furthermore, these ratios vary considerably from place to place, as would be expected for an unsaturated maser (but see below). (3) The strongest hyperfine component has a significantly narrower line width, according to MNBK, than the weaker components (see also McGee *et al.* 1975). This observation is qualitatively consistent with the line narrowing effects that accompany unsaturated maser amplification. (4) Although a total of 30 sources other than Sgr B2 have been searched for $J = 1 \rightarrow 0$ HC_3N emission (Turner 1971 and MNBK), none have been detected, and the upper limits are ~ 10 times less than the Sgr B2 intensity. If the $1 \rightarrow 0$ intensity is approximately proportional to the HC_3N abundance, then this line should have been detected elsewhere, notably Sgr (NH_3A). We conclude that a nonlinear process (i.e., exponential gain) is at work in Sgr B2. (5) As noted in § II, the velocity of peak emission intensity is somewhat larger for the $J = 2 \rightarrow 1$ and $J = 1 \rightarrow 0$ lines than for the other HC_3N lines observed. This difference is explicable if the two lowest lines are the result of maser action, since the velocity along the path of highest gain through the cloud in the $1 \rightarrow 0$ transition does not, in general, correspond to the velocity of maximum "thermal" emission in the high-lying lines. (6) The contours of integrated intensity of $1 \rightarrow 0$ HC_3N emission follow the contours of background continuum intensity fairly closely

(MNBK), as would be expected, since the background is presumably being amplified. (This might be fortuitous, because $5 \rightarrow 4$ intensity also has a similar distribution.) In any case, present evidence suggests that the continuum source is indeed behind the 62 km s^{-1} molecular cloud (Rogstad *et al.* 1975), although not necessarily behind all of the gas at lower velocities (50–60 km s^{-1}), where the higher lying HC_3N transitions have their maxima.

It is unlikely that the same excitation temperature applies to all three hyperfine components of the $1 \rightarrow 0$ transition for the following reason. An optical depth of -1.7 ± 0.5 in the main component is then needed to produce the observed hyperfine intensity *ratios*. But this large negative optical depth would (*a*) amplify the background to more than an order of magnitude larger than the observed 2 K, (*b*) still leave inexplicable abundance anomalies [a more likely value for $\tau(1 \rightarrow 0)$ is -0.2], and (*c*) mean that the ratio $T_b(H^{12}C^{12}C^{12}CN)/T_b(H^{12}C^{13}C^{12}CN) \approx 36$ reported by Gardner and Winnewisser (1975*b*) for the $1 \rightarrow 0$ line implies a much smaller abundance ratio, $[H^{12}C^{12}C^{12}CN]/[H^{12}C^{13}C^{12}CN] \leq 20$, which is unlikely. It thus appears that the excitation temperature is *not* the same for the three hyperfine components. This might occur if the $2 \rightarrow 1$ transition is inverted and is undergoing maser action, or, less likely, if a higher-lying transition is optically thick (see Kwan and Scoville 1975 for an analogous situation).

d) Other Sources

i) *Sagittarius* (NH_3A)

In view of the limited data, we have considered only single homogeneous cloud models for Sgr (NH_3A). A wide range of densities ($n_T = 10^{4.6 \pm 0.7}$ cm^{-3}) can account for the present observations; measurements of higher transitions ($J > 10$) are needed to narrow this range. If T_k is within a factor of 2 of 40 K, the opacities of all measured HC_3N transitions are small ($\tau < 0.2$), and $N(HC_3N) = (1.0 \pm 0.4) \times 10^{14}$ cm^{-3}. The abundance of HC_3N relative to H_2 molecules in this source can be derived by estimating a reasonable value for the depth of the cloud. Surveys of H_2CO (Scoville *et al.* 1972) and NH_3 (Kaifu *et al.* 1975) indicate that the Sgr A molecular cloud is extended at least along the galactic plane. If the cloud extends 8–20 pc along the line of sight (corresponding to 3′–7′ apparent distance for galactic center sources), then $[HC_3N]/[H_2] = 10^{-10.1 \pm 0.9}$. Note that a cloud diameter of 8 pc implies that the total cloud mass must be greater than $10^5\ M_\odot$.

ii) *Orion KL*

Of the two molecular components of KL discussed by Zuckerman and Palmer (1975), only the "spike" or "ridge" component is evident in HC_3N emission. Furthermore, a homogeneous, single component model is adequate for fitting the HC_3N data to within the uncertainties.

If we assume $T_k = 50$ K, the best-fitting model has $n_T = 10^{5 \pm 0.4}$ and $N(HC_3N) = (2.4 \pm 0.6) \times 10^{13}$ cm^{-2}. The optical depths are small ($\lesssim 0.02$) in all of the measured transitions. The total density in the model is in the same range as the density previously suggested for the "ridge" component (Evans *et al.* 1975; Liszt *et al.* 1974), which is consistent with our observation that HC_3N is extended along the ridge. If we use the projected density of H_2 molecules in the KL direction suggested by Evans *et al.* (1975) [$N(H_2) \approx 2 \times 10^{23}$ cm^{-2}], we derive a mean value of the relative abundance of cyanoacetylene in this source: $[HC_3N]/[H_2] = 10^{-9.8 \pm 0.5}$ (estimated maximum uncertainty).

iii) *Cloud 2*

A fairly wide range of physical conditions can account for the single observation of cloud 2, a dark dust cloud in Taurus. Measurements of other transitions (e.g., $J = 3 \rightarrow 2$) can narrow this range considerably. If $T_k \approx 10$ K, and if the cloud is ~ 1 pc thick, a set of parameters which reasonably accounts for our observation is the following: $n_T = 10^{4.5}$ cm^{-3}, $n(HC_3N)/n(H_2) = 10^{-9.5}$–$10^{-10}$, $N(HC_3N) \approx 1 \times 10^{13}$ cm^{-2}, and $\tau(J = 5 \rightarrow 4) \approx 1$. A total density as low as 10^3 cm^{-3} can conceivably produce the observed line, but only if the relative HC_3N abundance is about two orders of magnitude larger [$n(HC_3N)/n(H_2) = 10^{-7.8}$], in which case $N(HC_3N) \approx 5 \times 10^{13}$ cm^{-2}, $\tau(5 \rightarrow 4) \approx 3.6$, and trapping is of marginal importance. In any case, the opacity in the $5 \rightarrow 4$ line in cloud 2 is significantly higher than it is in Orion KL primarily because T_k is much lower in cloud 2, and therefore the population difference between successive levels is much larger. Also, at the higher T_k of KL, the total population is spread out over a greater number of levels.

iv) *W51*

The data for five lines in this source are too poor and inconsistent to attempt a detailed fit to a source model. The data suggest that the mean value of $n_T \gtrsim 10^{4.5}$, and that $N(HC_3N) = 10^{13.5 \pm 0.3}$.

IV. DISCUSSION AND CONCLUSIONS

The relative abundance of HC_3N in Orion KL ($F = N(HC_3N)/N(H_2) = 10^{-9.8 \pm 0.5}$) is representative of that for the few sources for which we have been able to make an estimate, with the exception of the core component of Sgr B2 ($F = 10^{-11 \pm 0.7}$). When the Sgr B2 core is considered along with other sources, there is a weak indication that F decreases with increasing total density between $n_T = 10^4$ and 10^6 cm^{-3}. This is possible if rates of chemical reactions that destroy HC_3N increase with density faster than the formation rates, or if the formation rate actually decreases with increasing density. In either case, more complex molecules are likely to result. Alternatively, HC_3N might readily condense onto grains at a rate that is proportional to density.

It is of interest to compare cyanoacetylene abundances with those of other known molecular species containing the CN radical: CH_3CN, HCN, and CN.

The molecule CH_3CN has been reported only for Sgr B2 and Sgr A (Solomon *et al.* 1971) with projected densities approximately the same as those of HC_3N. The abundances of HCN are uncertain because of the undetermined contribution of trapping, but it appears that the ratio $N(HCN)/N(HC_3N)$ varies considerably from about 2 in Orion KL to roughly a few tenths in Sgr B2. It is noteworthy that HC_3N appears more abundant than HCN in some dense clouds. Similar cloud-to-cloud variations of relative abundances occur for CN (cf. Turner and Gammon 1975). $N(CN)/N(HC_3N) \approx 10$ in Orion KL and W51, but is less than 0.1 in Sgr B2 and Sgr (NH_3A) (only upper limits on CN emission are available for these sources). Clearly, there are rather large variations in HC_3N/HCN/CN abundance ratios between clouds having various physical conditions, and thus it is not surprising that F, the relative HC_3N abundance, seems to vary as a function of density.

The dominant chemical formation process for HC_3N is not understood. Anders, Hayatsu, and Studier (1974) have demonstrated that HC_3N can form in catalytic reactions on grain surfaces, although their studies were limited to much higher temperatures than are characteristic of interstellar grains. Also, cyanoacetylene can conceivably form in a series of gas phase ion-molecule reactions. For example, a chain of reactions starting with $C^+ + HCN \rightarrow C_2N^+ + H$ and ending with a recombination reaction ($H_2C_3N^+ + e^- \rightarrow HC_3N + H$) can be constructed, but unfortunately the intermediate reaction rates and the stability of the exotic intermediate species are unknown. Such a chain would destroy HCN (and similarly CH_3CN) as HC_3N was formed, which is consistent with the large observed variation in the HCN/HC_3N ratio.

We have not included an infrared radiation field in our statistical equilibrium calculations, although it is possible that radiative excitation of the lowest lying excited vibrational state ($\sim 228\ cm^{-1}$) and the subsequent cascade to the ground state can tend to thermalize the rotational levels of the ground vibrational state (cf. Morris 1975) at the effective infrared temperature. This effect might be important in Sgr B2 and Orion KL, but the line strength for the transition to this vibrational state (a bending mode), while unknown, is likely to be small. Thus populations of HC_3N rotational levels are probably not significantly affected by the infrared fluxes where $n_T \gtrsim 10^3\ cm^{-3}$.

In summary, the advantages of HCCCN as a probe of interstellar clouds are the following: (1) it is widespread and found in many different types of objects; (2) many lines (~ 16), covering a large range of transition probabilities, are accessible to present radio-frequency equipment, (3) most of the lines are predicted to be optically thin; if this is the case, then our approximate and relatively simple interpretation suffices, and (4) the three ^{13}C-substituted species will eventually allow an additional check of $^{12}C/^{13}C$ isotope ratios. Furthermore, emission from high J transitions ($J \geq 12$) arises only in the dense cores of molecular clouds and might thus prove to be a valuable probe of regions where star formation is in progress.

We are grateful to L. J Rickard and N. Z. Scoville for use of their computer programs, and to N. J. Evans for helpful comments on the manuscript. Partial financial support for this research came from NSF grants MPS 73-05282 A01 to the University of Chicago, GP-26218 to the University of Maryland, MPS 72-05045 A2 to the California Institute of Technology, and from the Alfred P. Sloan Foundation.

REFERENCES

Anders, E., Hayatsu, R., and Studier, M. H. 1974, *Ap. J. (Letters)*, **192**, L101.
Cheung, A. C., Rank, D. M., Townes, C. H., Knowles, S. H., and Sullivan, W. T., III. 1969, *Ap. J. (Letters)*, **157**, L13.
Clark, F. O., Buhl, D., and Snyder, L. E. 1974, *Ap. J.*, **190**, 545.
DeZafra, R. L. 1971, *Ap. J.*, **170**, 165.
Dickinson, D. F. 1972, *Ap. Letters*, **12**, 235.
Evans, N. J., II, Zuckerman, B., Sato, T., and Morris, G. 1975, *Ap. J.*, **199**, 383.
Gardner, F. F., Ribes, J. C., and Sinclair, M. W. 1971, *Ap. J. (Letters)*, **169**, L109.
Gardner, F. F., and Winnewisser, G. 1975*a*, *Ap. J. (Letters)*, **195**, L127.
———. 1975*b*, *ibid.*, **197**, L73.
Goldreich, P., and Kwan, J. 1974, *Ap. J.*, **189**, 441.
Goldsmith, P. F. 1972, *Ap. J.*, **176**, 597.
Green, S., and Thaddeus, P. 1974, *Ap. J.*, **191**, 653.
Kaifu, N., Morris, M., Palmer, P., and Zuckerman, B. 1976, *Ap. J.*, in press.
Kwan, J., and Scoville, N. 1975, *Ap. J. (Letters)*, **195**, L85.
Liszt, H. S., Wilson, R. W., Penzias, A. A., Jefferts, K. B., Wannier, P. G., and Solomon, P. M. 1974, *Ap. J.*, **190**, 557.
McGee, R. X. 1970, *Australian J. Phys.*, **23**, 541.
McGee, R. X., Newton, L. M., Batchelor, R. A., and Kerr, A. R. 1973, *Ap. Letters*, **13**, 25 (MNBK).
McGee, R. X., Newton, L. M., and Butler, P. W. 1975, preprint.
Morris, M. 1975, *Ap. J.*, **197**, 603.
Morris, M., Gilmore, W., Palmer, P., Turner, B. E., and Zuckerman, B. 1975, *Ap. J. (Letters)*, **199**, L47.
Morris, M., Palmer, P., Turner, B. E., and Zuckerman, B. 1973*a*, *IAU Symposium, No. 52, Interstellar Dust and Related Topics*, ed. Greenberg and Van de Hulst, p. 381 (Paper I).
———. 1974, *Ap. J.*, **191**, 349.
Morris, M., Zuckerman, B., Palmer, P., and Turner, B. E. 1973*b*, *Ap. J.*, **186**, 501.
Righini, G., Simon, M., Joyce, R. R., and Gezari, D. Y. 1975, *Ap. J. (Letters)*, **195**, L77.
Rogstad, D. H., Lockhart, I., and Whiteoak, J. B. 1975, *Astr. and Ap.*, **36**, 253.
Scoville, N. Z., and Solomon, P. M. 1974, *Ap. J. (Letters)*, **187**, L67.
Scoville, N. Z., Solomon, P. M., and Thaddeus, P. 1972, *Ap. J.*, **172**, 335.
Snyder, L. E., and Buhl, D. 1971, *Ap. J. (Letters)*, **163**, L47.
Solomon, P. M., Jefferts, K. B., Penzias, A. A., and Wilson, R. W. 1971, *Ap. J. (Letters)*, **168**, L107.
Solomon, P. M., Penzias, A. A., Jefferts, K. B., and Wilson, R. W. 1973, *Ap. J. (Letters)*, **185**, L63.
Thaddeus, P., Kutner, M. L., Penzias, A. A., Wilson, R. W., and Jefferts, K. B. 1972, *Ap. J. (Letters)*, **176**, L73.
Tucker, K. D., Kutner, M. L., and Thaddeus, P. 1974, *Ap. J. (Letters)*, **193**, L115.
Turner, B. E. 1971, *Ap. J. (Letters)*, **163**, L35.
Turner, B. E., and Gammon, R. H. 1975, *Ap. J.*, **198**, 71.

Turner, B. E., Zuckerman, B., Palmer, P., and Morris, M. 1973, *Ap. J.*, **186**, 123.
Westenberg, A. A., and Wilson, E. B., Jr. 1950, *J. Am. Chem. Soc.*, **72**, 199.
Zuckerman, B., Morris, M., Turner, B. E., and Palmer, P. 1971, *Ap. J.* (*Letters*), **169**, L105.
Zuckerman, B., and Palmer, P. 1975, *Ap. J.* (*Letters*), **199**, L35.

M. MORRIS: Owens Valley Radio Observatory, California Institute of Technology, Pasadena, CA 91125
PATRICK PALMER: Department of Astronomy and Astrophysics, University of Chicago, Chicago, IL 60637
B. E. TURNER: National Radio Astronomy Observatory, Edgemont Road, Charlottesville, VA 22901
B. ZUCKERMAN: Astronomy Program, University of Maryland, College Park, MD 20742